

Defect Structures of Tin-Doped Indium Oxide

Oliver Warschkow,[†] Donald E. Ellis,^{*,†} Gabriela B. González,^{*,‡} and Thomas O. Mason^{*,‡}Department of Physics and Astronomy and Institute of Environmental Catalysis, and
Department of Materials Science and Engineering, Northwestern University, Evanston, Illinois 60208

Defect structures associated with tin doping of indium oxide, an optically transparent conductor, have been characterized by atomistic simulations and first-principles density functional calculations. A comprehensive survey of defect clusters containing up to three tin dopants in the first and second cationic coordination shells of an oxygen interstitial has been conducted. The analysis of energetically favorable defects gives insights into the role and nature of defect clusters in the material. In particular, the origins of the experimentally postulated b-site preference of tin dopants have been examined. Our results show that b-site preference occurs only in defect clusters with oxygen interstitials and is not intrinsic to dopants. In contrast, in nearest coordination to an interstitial, a strong d-site preference is found. Density functional calculations in the discrete variational-embedded cluster approximation have been conducted on selected defect structures to illuminate the effect of clustering on partial atomic charges, bond-orders, and ¹¹⁹Sn Mössbauer parameters.

I. Introduction

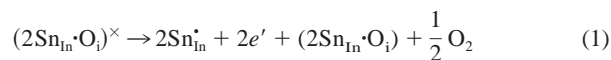
TIN-DOPED INDIUM OXIDE (Sn-In₂O₃, ITO) is a transparent conductor frequently used in devices such as computer displays and touch screens and as functional layers in optoelectronic components. Its electronic and optical properties are critically dependent on the presence and distribution of the tin electron donors, local chemistry, and charge balance of the related defect sites. Efforts to optimize fabrication, performance, and lifetime of this and related transparent conductors depend on an understanding of atomic-scale properties.¹

Pure In₂O₃ crystallizes in a large cubic bixbyite-type unit cell (space group No. 206, *Ia*₃, *a* = 10.117 Å), which contains 80 atoms or 16 formula units.² In₂O₃ structure is related to a 2×2×2 supercell of fluorite, in which one-fourth of all anion sites are structurally vacant. These vacant sites provide the space to accommodate excess, that is, interstitial, oxygen atoms, which are of major interest in this work. Depending on the relative positioning of structural vacancies, two types of indium sites exist in the unit cell, termed b- and d-sites in Wyckoff notation, of which there are 8 and 24, respectively, in the unit cell.³ All 48 oxygen sites (Wyckoff 48f) in the unit cell are symmetry equivalent, as are the 16 interstitial sites (Wyckoff 16c). Both types of indium sites are sixfold coordinated by oxygen in a distorted octahedral geometry, of which the b-site is somewhat more regular. In turn, all oxygen

sites (actual as well as structurally vacant sites) are coordinated by four indium atoms, one In(b) and three In(d).

According to the anion interstitial defect model (Subbarao *et al.*⁴), ITO can be expressed as In_{2-δ}Sn_δ(O_i)_{δ/2} using Kröger–Vink notation. In this model, all cation sites are filled. Because of the smaller ionic radius of tin (*r* = 0.71 Å) as compared with that of indium (*r* = 0.81 Å), tin can substitute into the indium sites. Because the dopant substitutes as Sn⁴⁺ (Köstlin *et al.*⁵), the replacement of δ Sn⁴⁺ for In³⁺ creates a charge imbalance that is compensated by the formation of δ/2 O_i[•] anions that occupy some of the structural anion vacancy sites of In₂O₃.

From measured electrical properties of ITO thin films (conductivity, carrier density, and mobility as a function of tin content and oxygen partial pressure (*p*_{O₂})), Frank and Köstlin⁶ have deduced the existence of associated neutral defects (2Sn_{In}•O_i)[×] whose concentration depends on *p*_{O₂} and tin content. The primary argument follows (see Refs. 6 and 7 for a discussion). During reduction of these associated defects,



Sn_{In}[•] are freed and charge compensated by electrons, resulting in an increased conductivity in reduced ITO materials. The mass action law for this reaction

$$K = \frac{p_{\text{O}_2}^{1/2}[\text{Sn}_{\text{In}}^{\bullet}]^2 n^2}{[(2\text{Sn}_{\text{In}}\cdot\text{O}_i)^{\times}]} \quad (2)$$

combined with the charge neutrality condition *n* = [Sn_{In}[•]] yields the following expression for the carrier density *n*:

$$n = K[(2\text{Sn}_{\text{In}}\cdot\text{O}_i)^{\times}]^{1/4} p_{\text{O}_2}^{-1/8} \quad (3)$$

which explains the experimentally found *p*_{O₂}^{-1/8} dependence as well as the total tin concentration [Sn_{tot}]^{1/4} dependence in the limit of high *p*_{O₂} (at which Sn is mostly in [(2Sn_{In}•O_i)[×]]). Under strongly reducing conditions, with the balance of Eq. (1) very much on the right-hand side, the carrier concentration is proportional to the total tin concentration. To explain deviations from these dependencies at higher tin level (>3%, depending on *p*_{O₂}), Frank and Köstlin⁶ have further introduced so-called nonreducible defects made up of “inactive” tin ions that remain nonionized, even in highly reducing conditions.

Nadaud *et al.*⁸ and González *et al.*⁹ have used Rietveld refinement on powder neutron diffraction data to obtain structural information about ITO materials as a function of *p*_{O₂} and tin doping. The Rietveld results agree with Mössbauer experiments,^{8,10} which show a preference of tin for occupying the b- rather than the d-site. In a 4.5-cation%-Sn ITO, the fraction of Sn on b-sites is 0.118(37), while the d-site has a fractional occupancy of only 0.018(17).⁹ Also, interstitial oxygen anions are present in all ITO samples and absent in the pure In₂O₃ samples.⁹

Studies of the electronic structure of ITO include optical spectroscopy¹¹ and X-ray photoemission studies,¹² establishing an experimental understanding of the energy-band structure of the material in good agreement with electronic structure calculations. Assorted density functional calculations have been published on In₂O₃ in bulk form as well as containing a single tin dopant:

J. Tanaka—contributing editor

Manuscript No. 186700. Received August 3, 2002; approved May 12, 2003.
Supported in part by the U.S. Department of Energy, under Grant No. DE-FG02-84ER45097. OW supported by the EMSI program of the National Science Foundation and the U.S. Department of Energy Office of Science (CHE-9810378) at the Northwestern University Institute for Environmental Catalysis.

^{*}Member, American Ceramic Society.[†]Department of Physics and Astronomy and Institute of Environmental Catalysis.[‡]Department of Materials Science and Engineering.

LMTO-ASA calculations by Odaka and co-workers,^{13,14} embedded cluster DV-X α calculations by Tanaka *et al.*,¹⁵ and FLMTO calculations by Myrasov and Freeman¹⁶ report band structure calculations for ITO, modeled as an In₂O₃ unit cell with 1/16 of indium sites substituted by tin, thus approximating 6.5% tin doping. Myrasov and Freeman report a small energetic preference (0.05 eV) for a tin atom substituting at the b-site over the d-site, in apparent agreement with experiment.^{7–9} To our knowledge, no electronic structure calculations have been reported that go beyond isolated point defects to address clustered defects.

The objective of this work is to use theoretical methods to further expand our understanding of the complex defect chemistry of ITO. Atomistic simulations are used to determine the local geometry and energetics of defect clusters containing one to three tin dopant atoms around a single oxygen interstitial. Selected defect structures are further examined by first-principles embedded cluster density functional methods to reveal electronic charge distributions to be correlated with available Mössbauer spectroscopic data. From these calculations, we seek a microscopic, atomic-level understanding of cluster structure and formation from which to rationalize the macroscopic properties of ITO. As such, this work is complementary to experiment, which has—by and large—deduced ITO atomic-scale properties, such as the nature of the (2Sn_{in}O_i)^x cluster, from measured macroscopic and, thus, atomic-scale, statistically averaged properties. An in-depth discussion of the nature of the nonreducible cluster in the Frank and Köstlin model⁶ from the perspective of the model used in this work is the subject of a separate article.¹⁷

II. Models and Methodology

(I) Atomistic Potential Model

All structural, lattice, and defect energies reported in this work have been calculated using the atomistic Born model of polar solids, as implemented by the GULP package.^{18,19} Lattice ions are represented as point ions, and all interactions between ions are assumed to be pairwise, consisting of Coulombic, Pauli-repulsion, and dispersion forces. The latter two are modeled using the well-known Buckingham-potential form,

$$\phi_{ij}(r) = A_{ij} \exp(-r/\rho_{ij}) - \frac{C_{ij}}{r^6} \quad (4)$$

where A_{ij} , ρ_{ij} , and C_{ij} are parameters particular to each pair of atom types. In addition, oxide ions are allowed to polarize by means of the shell model;²⁰ i.e., each oxide ion is represented by a pair of point charges (core and shell) attached to each other by a spring potential. The parameter set for O–O interactions was taken from the library of oxide potentials reported by Bush *et al.*,²¹ which was derived by fitting to a wide range of oxide lattice structures as well as elastic and dielectric constants. The Sn–O interaction parameters were based on those reported by Freeman and Catlow;²² however, to make this parameter set compatible with the Bush *et al.* O–O potential, it was refitted by us to experimental SnO₂ lattice parameters using GULP procedures. Similarly, the In–O parameter set was based on a potential reported by McCoy *et al.*²³ for In₂O₃, which we also refitted for compatibility with the Bush *et al.* O–O potential. For convenience, we have summarized in Table I the full set of interaction parameters used in this work. All potentials were derived from binary oxides. To ascertain the transferability of these potentials to systems of mixed stoichiometry, we performed

Table I. Potential Parameters Used in Work[†]

Interaction	A (eV)	ρ (Å ⁻¹)	C (eV/Å ⁶)	Reference
In ³⁺ –O ²⁻	2719.77	0.2917	0.0	This work
Sn ⁴⁺ –O ²⁻	2180.89	0.3076	0.0	This work
O ²⁻ –O ²⁻	25.41	0.6937	32.32	Bush <i>et al.</i> ²¹

[†]Oxygen-anion shell-model potentials are $Y(e) = -2.513e$ and $k = 20.53 \text{ eV/Å}^2$.²¹ All short-range potentials are cut off of at 12 Å.

a lattice structure optimization for the tertiary oxide In₄Sn₃O₁₂, for which an experimental structure was reported by Nadaud *et al.*⁸ Table II shows that the agreement between calculated and experimental structure is excellent.

Defect energies have been calculated using the Mott–Littleton²⁴ procedure as implemented in the GULP package,^{18,19} which yields defect energies in the limit of infinite dilution. Two cutoff radii r_I and r_{II} divide space into three regions. In the innermost region ($r < r_I$), all atoms are allowed to relax explicitly; beyond, the effect of atomic relaxations on the defect energy is treated in an increasingly approximate fashion. In this work, the cutoff radii r_I and r_{II} have been chosen as large as computationally practical (12 and 22 Å, respectively).

In this work, we focus on clusters formed by coordination of one or more Sn_{in} point defects around a given oxygen interstitial. Out of computational expediency, we limit our survey to tin substitution in the first and second cationic shells around O_i. We are primarily interested here in defect cluster formation energies, which are defined as the energy gain or loss of forming a cluster from isolated point defects in reaction patterns that can be formulated as



The objective of this survey is then to identify and distinguish favorable (i.e., relatively stable) cluster structures from other, less stable arrangements. For cluster formation energies, the defect energies of the isolated, that is, nonclustered, point defects O_i and Sn_{in} serve here as the reference point. These reference energies are listed in Table III.⁸

In this model, calculated formation energies (and reaction energies in general) do not consider the effect of entropy, which is beyond the scope of this work. Qualitatively, the effect of entropy at high temperature is to act against aggregation of point defects into clusters.

In its first, nearest-neighbor coordination shell, an O_i^o interstitial site is coordinated by four cations (one b-site and three d-sites). The second cationic coordination shell contains 12 indium atoms (three b-sites and nine d-sites) at distances of 3.9–4.2 Å (assuming bulk structure) from the interstitial site (see Fig. 1(b)). In the following, we use in our cluster notation a vertical bar (|) to distinguish atoms in the first and second shell around O_i^o. We further denote tin substitution at indium b- and d-sites simply as Sn(b) and Sn(d), respectively, omitting the superfluous In subscript of the Kröger–Vink notation. Three classes of defects have

⁸We wish to point out here—because this is often not clear to those unfamiliar with Mott-type defect calculation—that relative stability of defects can be deduced only from such energies if they are of the same stoichiometry. Therefore, we can, in Table III, make a comparison between Sn(b) and Sn(d) in terms of relative stability, but cannot directly compare the stability of an O_i^o and Sn(b) or Sn(d) unless an account is taken of the stoichiometry difference.

Table II. Experimental and Calculated Structure of In₄Sn₃O₁₂

Parameter	Axis	Structure	
		Experiment [†]	Calculated [‡]
Lattice parameter	a (Å)	9.4604	9.4635
	c (Å)	8.8584	8.7714
Cation 1 [§]	$x = y = z$	0	0
Cation 2 [¶]	x	0.2526	0.2517
	y	0.2145	0.2124
	z	0.3497	0.3490
O1	x	0.1979	0.1993
	y	0.1768	0.1737
	z	0.1162	0.1150
O2	x	0.1886	0.1900
	y	0.9745	0.9733
	z	0.3917	0.3964

[†]Nadaud *et al.*⁸ [‡]This work. [§]100% Sn. [¶]33% Sn, 66% In.

Table III. Defect Energies of Relevant Point Defects in In_2O_3 and Geometric Relaxation Contribution to the Defect Energy

Defect	Defect energy (eV)	Relaxation energy [†] (eV)
$\text{Sn}(\text{b})^*$	-35.47	0.89
$\text{Sn}(\text{d})^*$	-35.52	0.77
O_i''	-10.85	5.36

[†]Stabilization that a point defect gains by the local positional relaxation of the atoms surrounding it.

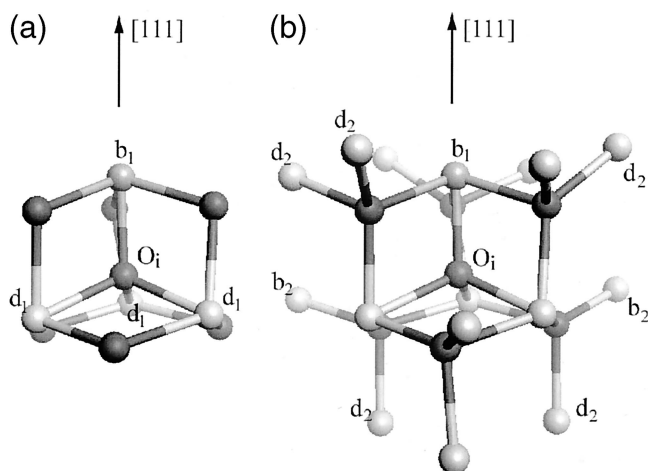


Fig. 1. (a) Eleven-atom structural core of the 38-atom quantum clusters used in the DVM calculation of partial atomic charges and ^{119}Sn Mössbauer isomer shifts and quadrupole splittings. Displayed is the central O_i site tetrahedrally coordinated by four indium and six structural oxygen atoms. Indexes b_1 and d_1 denote b-type and d-type indium sites in the first cationic coordination shell around O_i , respectively. (b) Extended cluster showing the positions of second-shell cations around O_i . Indexes b_2 and d_2 distinguish lattice b- and d-site cations in the second shell. There is a threefold rotation axis along the O_i - b_1 axis.

been considered: (i) nearest-neighbor clusters ($n\text{Sn}\cdot\text{O}_i$) with all combinations of up to $n = 4\text{Sn}_{\text{In}}$ substitutions in the first coordination shell; (ii) next-nearest-neighbor clusters ($n\text{Sn}|\text{O}_i$) with up to $n = 3\text{Sn}$ in the second cationic coordination shell; and (iii) mixed clusters ($n\text{Sn}/m\text{Sn}\cdot\text{O}_i$) with partial Sn substitution of up to $n + m = 3\text{Sn}$ in the first and second coordination shells. Our survey for these classes of defects is comprehensive in that structure relaxations and defect energy calculations have been performed for all positional combinations.

For the seven combinations of nearest-neighbor defect clusters ($n\text{Sn}\cdot\text{O}_i$), defect formation energies are listed in Table IV. The data are consolidated with those for the other clusters, ordered by defect cluster stabilization energy and grouped by defect stoichiometry in Table V. Because of the many combinations, formation energies of only the most stable in a series are reported. Obviously, the energies of clusters within a given series vary because of the relative positioning of tin atoms.

(2) Density Functional Scheme

Density functional theory (DFT) provides a robust first-principles approach²⁵ to analyze the electronic structure of materials, which has been widely applied in study of molecules and solids.²⁶ Band structure methodologies and localized orbital cluster schemes have been developed that are adequate to treat complex systems, as described in recent reviews.²⁷ In this work, we make use of an embedded cluster density functional (ECDF) implementation, which treats a finite fragment self-consistently embedded in the potential field of the infinite host.^{28,29} A brief sketch of the method follows. A

Table IV. Cluster Formation Energies of Nearest-Neighbor Defect Clusters of Sn_{In} and O_i

Defect cluster	Cluster formation energy [†] (eV)
$(\text{Sn}(\text{b})\cdot\text{O}_i)'$	-0.89
$(\text{Sn}(\text{d})\cdot\text{O}_i)'$	-1.29
$(\text{Sn}(\text{b})\cdot\text{Sn}(\text{d})\cdot\text{O}_i)^\times$	-1.54
$(2\text{Sn}(\text{d})\cdot\text{O}_i)^\times$	-1.91
$(\text{Sn}(\text{b})\cdot 2\text{Sn}(\text{d})\cdot\text{O}_i)^*$	-1.49
$(3\text{Sn}(\text{d})\cdot\text{O}_i)^*$	-1.86
$(\text{Sn}(\text{b})\cdot 3\text{Sn}(\text{d})\cdot\text{O}_i)^{**}$	-0.88

[†]With respect to isolated O_i and $\text{Sn}(\text{d})$ defect energies (Table III).

numerical atomic orbital DFT basis set is generated, defined in terms of atomic configurations generated from Mulliken population analysis of the self-consistent field (SCF) cluster potential. The iteration process is begun by constructing a total density (charge and spin density) ρ as a sum of cluster valence and core densities and that of the external host environment. The Coulomb potential V_C and exchange-correlation potential V_{xc} are constructed, using a least-squares expansion of ρ in terms of auxiliary functions. Matrix elements of the DF Hamiltonian \mathbf{H} and overlap \mathbf{S} are formed over the basis set, and the matrix secular equation $(\mathbf{H} - \epsilon\mathbf{S})\mathbf{C} = 0$ is solved to obtain expansion coefficients \mathbf{C} of the cluster eigenstates in terms of the basis set. A new cluster density is formed using Fermi-Dirac occupation numbers n_i

$$\rho_{\text{cluster}} = \sum_i n_i |\psi_i|^2 \quad (6)$$

and combined with the host density to begin a new SCF cycle. The SCF iterations are terminated when a desired level of precision in

Table V. Overview of Defect Clusters of One to Three Sn_{In} Substitutions in the First and Second Cationic Shells around an Oxygen Interstitial Site O_i [†]

$\text{Sn}:\text{O}_i$ ratio	Most stable defect clusters	Cluster formation energy (eV)
1:1 [$\text{Sn}\cdot\text{O}_i$]'	$(\text{Sn}(\text{d})\cdot\text{O}_i)'$	-1.29
	$(\text{Sn}(\text{b}) \text{O}_i)'$	-1.16
	$(\text{Sn}(\text{d}) \text{O}_i)'$	-1.10
	$(\text{Sn}(\text{b})\cdot\text{O}_i)'$	-0.89
2:1 [$2\text{Sn}\cdot\text{O}_i$] [×]	$(\text{Sn}(\text{b}) \text{Sn}(\text{d})\cdot\text{O}_i)^\times$	-2.09
	$(2\text{Sn}(\text{b}) \text{O}_i)^\times$	-2.08
	$(\text{Sn}(\text{d}) \text{Sn}(\text{d})\cdot\text{O}_i)^\times$	-2.05
	$(\text{Sn}(\text{b})\text{Sn}(\text{d}) \text{O}_i)^\times$	-2.00
	$(2\text{Sn}(\text{d}) \text{O}_i)^\times$	-1.97
	$(2\text{Sn}(\text{d})\cdot\text{O}_i)^\times$	-1.91
	$(\text{Sn}(\text{d}) \text{Sn}(\text{b})\cdot\text{O}_i)^\times$	-1.63
	$(\text{Sn}(\text{b}) \text{Sn}(\text{b})\cdot\text{O}_i)^\times$	-1.54
	$(\text{Sn}(\text{b})\cdot\text{Sn}(\text{d})\cdot\text{O}_i)^\times$	-1.54
	Dissociation: [$\text{Sn}\cdot\text{O}_i$]' + Sn^*	-1.29
3:1 [$3\text{Sn}\cdot\text{O}_i$]'	$(3\text{Sn}(\text{b}) \text{O}_i)^*$	-2.55
	$(2\text{Sn}(\text{b})\cdot\text{Sn}(\text{d}) \text{O}_i)^*$	-2.43
	$(\text{Sn}(\text{b})\cdot 2\text{Sn}(\text{d}) \text{O}_i)^*$	-2.36
	$(2\text{Sn}(\text{b}) \text{Sn}(\text{d})\cdot\text{O}_i)^*$	-2.35
	$(3\text{Sn}(\text{d}) \text{O}_i)^*$	-2.33
	$(\text{Sn}(\text{b})\cdot\text{Sn}(\text{d}) \text{Sn}(\text{d})\cdot\text{O}_i)^*$	-2.31
	$(2\text{Sn}(\text{d}) \text{Sn}(\text{d})\cdot\text{O}_i)^*$	-2.24
	$(\text{Sn}(\text{d}) 2\text{Sn}(\text{d})\cdot\text{O}_i)^*$	-2.14 [‡]
	Dissociation: [$2\text{Sn}\cdot\text{O}_i$] [×] + Sn^*	-2.09
	$(2\text{Sn}(\text{d}) \text{Sn}(\text{b})\cdot\text{O}_i)^*$	-1.88 [§]
$(3\text{Sn}(\text{d})\cdot\text{O}_i)^*$	-1.86 [¶]	

[†]Defect clusters are grouped by stoichiometry $\text{Sn}_{\text{In}}:\text{O}_i$ and ordered by cluster formation energy, such that the energetically most stable clusters appear near the top of the respective stoichiometry group. Each row refers to a series of defect clusters differing in the relative positioning of Sn_{In} around the interstitial site (see text). All energies refer to the most stable arrangement in a given series and are with respect to isolated O_i and $\text{Sn}(\text{d})$ defect energies (Table III). [‡]Most stable 3:1 cluster with two Sn_{In} substitutions in the first shell. [§]Most stable 3:1 cluster with a $\text{Sn}(\text{b})$ substitution in the first shell. [¶]Most stable 3:1 cluster with three Sn_{In} substitutions in the first shell.

density and potential has been achieved. Optimization of the basis set forms a supercycle of the SCF procedure. The cluster wave functions and energies ψ_i , ϵ_i , and density ρ are then used as input to various analyses, including spectroscopic densities of states, optical and X-ray absorption profiles, electron energy-loss spectra, and cohesive energy. Bond order analysis and contour maps of electron density prove to be useful in interpreting bonding mechanisms.

In this work, the Mulliken atomic charges and Mössbauer calculations were performed on relaxed defect structures obtained from the atomistic calculations. The DFT equations were explicitly solved for clusters of 37 and 38 atoms (depending on whether the O_i' site was occupied) embedded into the effective potential of more than 500 surrounding lattice atoms. To achieve a maximum of internal consistency, all clusters were geometrically centered on the O_i' site. This site is coordinated by four indium sites (one In(b) and three In(d) sites) in the first shell, and six structural oxygen atoms in the second shell. These 11 atoms make the core of the quantum cluster that is displayed in Fig. 1. The full 37/38-atom cluster consists of all first-shell coordinating atoms to any one atom in this core cluster.

Mössbauer isomer shifts and quadrupole splitting can be calculated, respectively, from the electron density and electric-field gradient at the nucleus. The isomer shift (IS) relative to SnO_2 is calculated using the calibration of Terra and Guenzburger;³⁰ i.e.,

$$\text{IS} = \alpha(\rho(0) - \rho(\text{SnO}_2)) \quad (7)$$

with $\alpha = 0.192(\text{mm/s})a_0^3$.

For the 28.8 keV transition of ^{119}Sn , the Mössbauer quadrupole splitting (QS) is related to the principal component V_{zz} and asymmetry parameter η of the electric-field-gradient tensor by

$$\text{QS} = \beta Q V_{zz} \left(\frac{1 - \eta^2}{3} \right)^{1/2} \quad (8)$$

where $\beta = -1.10$ and $Q = -0.109$ barn (1 barn = 10^{-24} $\text{cm}^2/\text{nucleus}$) and V_{zz} is in units of e/a_0^3 .³¹

III. Results and Discussion

(I) Atomistic Model: Defect Energies

Experimentally, the b-site preference of tin in ITO appears quite well established.^{8–10} This preference, however, is not borne out if we simply look at the calculated energies of the isolated Sn(b) and Sn(d) point defects (Table III). Numerically, the Sn(d) defect energy is slightly lower, that is, more stable, than Sn(b); however, the energy difference of 0.05 eV found here is too small for us to make a claim on preference with any amount of confidence, considering that various choices in the computational setup (defect cutoff radii, location of defect center) cause an uncertainty that we estimate at ~ 0.1 eV. The only other defect calculation on ITO of which we are aware is the first-principles FLMTD work of Myrasov and Freeman,¹⁶ who found a 0.05 eV preference for Sn(b). However, the Myrasov and Freeman result did not take local geometry relaxation into account; therefore, its accuracy is limited. In our model (Table III), the relaxation contribution to the defect energy alone amounts to 0.89 and 0.77 eV for Sn(b) and Sn(d) sites, respectively, more than an order of magnitude larger than the stipulated defect energy difference; thus, it is clearly a very relevant factor in the determination of site preference. The Myrasov and Freeman study and our calculation obviously agree on the smallness of the energy difference between Sn(b) and Sn(d), in qualitative agreement with experiment in so far that both types of defects are found to coexist in actual samples; the calculated energy difference, however, is too small to conclusively confirm the significantly higher occupancy found experimentally for the Sn(b) site.^{8,9} This can be resolved if we propose that b-site preference in ITO is associated with defect clustering.

Experimental evidence^{6,7} suggests that substantial clustering of Sn_{In} and O_i occurs in ITO. On mere qualitative arguments, the attraction of Sn_{In} into the vicinity of O_i makes sense for the

following reasons: First, the formally positively charged Sn_{In} defect provides charge compensation to the negatively charged O_i , and, second, the smaller Sn^{4+} ion can help to counter the ion-packing stress caused by the lattice having to accommodate the interstitial. Looking now at our results for defect clusters with Sn_{In} substitution in the first shell around O_i' (Table IV), we find tin substitution at the three d-sites strongly favored over substitution at the single b-site, quite unlike what has been found for isolated Sn(b) and Sn(d) defects (Table III). In all cases, an energy gain of ~ 0.35 eV can be made by moving a tin atom from the one b-site to any of the three d-sites. Taking a different perspective, an increase of the oxygen coordination from six to seven is apparently better tolerated by tin on a d-site than on a b-site. Within the subseries of nearest-neighbor clusters ($n\text{Sn}\cdot O_i$) ($n = 1, 2, 3$, and 4) with tin d-site occupation maximized, cluster stabilization energies are -1.29 , -1.91 , -1.86 , and -0.88 eV, respectively; thus, we find strong preference for nearest-neighbor arrangements of 2Sn(d) and 3Sn(d) around an O_i site relative to the isolated point defects.

Expanding the view and looking further at clusters with tin substituting in the first and second cationic shells around O_i (Table V), we can see that some of the clusters are a little more stable than the nearest-neighbor clusters, but the energy gain from nearest-neighbor to next-nearest-neighbor clusters is fairly small in comparison with the energy gained by clustering. For defect clusters of $\text{Sn}\cdot O_i$ stoichiometry of 2:1, the most stable of the next-nearest-neighbor clusters is $(\text{Sn}(\text{b})|\text{Sn}(\text{d})\cdot O_i)^\times$ with one d-site tin in the first and one b-site tin in the second cation shells. Table V also shows that the strong d-site preference observed for the first shell (Table IV) does not carry over into the second shell; e.g., $(\text{Sn}(\text{b})|O_i)$ and $(\text{Sn}(\text{d})|O_i)$ exhibit a stability difference of only 0.06 eV in favor of the former, again too small to determine a clear preference. Indeed, for the other stoichiometries of second- and mixed-shell clusters, there is a now substantial participation of b-site tin in low-energy clusters, and a clear d-site preference exists only when tin substitution occurs in the first shell.

As mentioned, the energies in Table V refer to the most stable structure in a series of defect clusters with different relative positioning of Sn_{In} around O_i . Closer inspection of favored and unfavored structures within the various series further reveals the following structural preferences.

(1) As noted above, Sn(b) in nearest coordination to O_i is unfavored. We found this rule universally confirmed in all 1:1, 2:1, and 3:1 defect cluster combinations.

(2) For defect clusters of 2:1 and 3:1 stoichiometries, two Sn_{In} at nearest cation positions relative to each other are a unfavored arrangement unless at least one of them (by rule 1 above, a d-site Sn_{In}) is also in nearest coordination to an O_i . Mutual electrostatic repulsion of the formally positive-charged Sn_{In} sites is the likely driving force. The exception is illustrated by two structures of the $(\text{Sn}(\text{b})|\text{Sn}(\text{d})\cdot O_i)^\times$ series of clusters with Sn(d) in nearest coordination to O_i . The most stable arrangement in the series—and, in fact, the whole 2:1 stoichiometry group—has Sn(b) in nonnearest cation position relative to the Sn(d) site; the structure with Sn(b) in nearest position to Sn(d) is only by 0.1 eV less stable.

(3) For possibly the same reason, in defect clusters of 2:1 and especially 3:1 stoichiometry, favored structures have a maximum of one Sn_{In} (again, a d-site) in the first shell around O_i . Whereas defect clusters with one Sn(d) in the first shell are generally of similar energy than comparable all-second-shell clusters, the most stable defect clusters with two Sn_{In} in the first shell are by 0.18 and 0.41 eV less stable than the most stable cluster overall in stoichiometries 2:1 and 3:1, respectively (Table V).

(4) For the 3:1 stoichiometry, there is a preference for structures where the three Sn_{In} sites form a regular triangle with the O_i site in the center. Clearly, for such a structure, the three dipoles between O_i and Sn_{In} cancel, and electrostatic stability is gained. In particular, the $(3\text{Sn}(\text{b})|O_i)'$ defect cluster, the most stable in the 3:1 set of clusters, is characterized by such a planar triangular structure in the $\langle 111 \rangle$ plane (see Fig. 1).

In ionic systems, where local coordination preferences are often transferable, we expect these empirical rules to be applicable to

other, more extensive defect clusters in ITO not covered by our survey as well as to related materials.

The discussion thus far has focused on the comparative energetics of isolated defect clusters within the three stoichiometry groups $\text{Sn}_{\text{In}}:\text{O}_i$ of 1:1, 2:1, and 3:1 composition. To make statements about the prevalence of one type of cluster over another in a particular ITO sample, we begin with a thermodynamic analysis for which we formulate reactions that convert clusters of differing composition into one another. The energies of reaction, calculable from the defect energies in Table V, then indicate where the balance rests. The key parameter in this is balance is the prevailing doping ratio $\text{Sn}_{\text{In}}:\text{O}_i$ of the ITO sample as a whole, that is, the relative concentration of oxygen interstitials and tin dopants (clustered or nonclustered) in the indium oxide lattice. In the formulation of these reaction energies, we use the cluster stabilization energies of the most stable cluster of a given stoichiometry. In the following, we use square brackets to refer to the energetically most stable cluster (see Table V).

On grounds of systematics, we begin with a hypothetical 1:1-doped ITO:



The macroscopic doping level is reflected in the stoichiometry of these equations. Equation (10), for example, illustrates that the presence of a $[2\text{Sn}\cdot\text{O}_i]^\times$ in a 1:1-doped material requires an isolated O_i' for mass conservation and that the system can gain energy by converting those two species to two $[\text{Sn}\cdot\text{O}_i]'$ clusters. Together, Eqs. (9) and (10) demonstrate the thermodynamic preference to form 1:1 defect clusters $[\text{Sn}\cdot\text{O}_i]'$.

Turning now to a more relevant ITO sample with a macroscopic doping ratio of 2:1, the typical ratio under which tin presumably enters the In_2O_3 lattice, we have the following reactions expressing the thermodynamic balance:

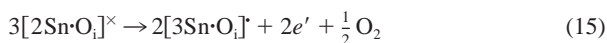


As is evident from these relations, the balance clearly favors neutral 2:1 defect clusters, and we should expect Eq. (13) to be the predominant equilibrium defect under these doping conditions, very much in agreement with the conventional understanding.⁶

When a 2:1-doped ITO sample is subjected to reducing conditions, oxygen interstitials are removed from the lattice, and the macroscopic $\text{Sn}_{\text{In}}:\text{O}_i$ ratio increases. For a ratio of 3:1, we consider the following reaction:



where we find that thermodynamics favors positively charged 3:1 clusters over neutral 2:1 clusters and isolated Sn_{In}^* . Therefore, as 2:1-doped ITO is reduced, that is, as $(2\text{Sn}_{\text{In}}\cdot\text{O}_i)^\times$ defect clusters are decomposed according to the Frank and Köstlin⁶ model and Eq. (1), we expect that the two Sn_{In}^* freed in the process are incorporated into other 2:1 clusters to form 3:1 clusters. Thus, the net reaction of reduction becomes



In analogy to the argument made above (see Eqs. (1)–(3)), we obtain, for the so-modified reaction, the following expression for the carrier density:

$$n = K[(2\text{Sn}_{\text{In}}\cdot\text{O}_i)^\times]^{3/4} p_{\text{O}_2}^{-1/8} \quad (16)$$

Equation (16) reveals that, at high p_{O_2} (i.e., tin mostly in the form of $[(2\text{Sn}_{\text{In}}\cdot\text{O}_i)^\times]$), the reaction in Eq. (15) gives an incorrect $n \propto [\text{Sn}_{\text{tot}}]^{3/4}$ dependence and not the correct $n \propto [\text{Sn}_{\text{tot}}]^{1/4}$ as does Eq. (1). Thus, we find that the thermodynamically favored reaction

(Eq. (15)) does not agree with what is actually found in experiment.⁶ The most likely source of this disagreement is kinetics: In fact, Sn_{In} —unlike O_i' —is probably immobile in the In_2O_3 lattice. Because of this, a reduction according to Eq. (15) under the formation of 3:1 clusters can occur at higher tin-doping levels, with the participating $[2\text{Sn}\cdot\text{O}_i]^\times$ in sufficiently close proximity. It is only under these conditions that we should expect the formation of a significant number of 3:1-type defects. At low tin-doping levels, with $[2\text{Sn}\cdot\text{O}_i]^\times$ positioned few and far between, the primary path of reduction remains by Eq. (1).

We conclude the following from Eqs. (9)–(16).

(1) Clustering of up to three Sn_{In} around a single O_i site is energetically favored (Eqs. (9), (11), and (14)); thus, we should expect substantial clustering of Sn_{In} and oxygen interstitials. The energy gain becomes smaller with every Sn_{In} added as the mutual electrostatic repulsion between formally positive Sn_{In} sites comes into effect. A noncomprehensive sampling of 4:1 clusters shows no increased binding with respect to 3:1 clusters. At low tin-doping levels, low Sn_{In} mobility probably prevents the formation of the thermodynamically favored clusters.

(2) In addition, Eqs. (10), (12), and (13) illustrate a general preference to distribute Sn_{In} over available oxygen interstitials (clustered and nonclustered), thus maximizing the amount of O_i' incorporated into any sort of defect cluster and—within clusters—minimizing the mutual electrostatic repulsion between Sn_{In} sites. This further acts as a lever of cluster size within a given doping ratio: For ratios up to 3:1, the reaction energies indicate a strong thermodynamic preference to form clusters that reflect the macroscopic doping ratio of the sample.

From the combination of these two trends—energy gain by clustering up to three Sn_{In} around O_i plus energy gain by distributing Sn_{In} over available O_i' —it is plausible that further stabilization is possible through further aggregation of, say, two $[2\text{Sn}\cdot\text{O}_i]^\times$ clusters into larger defect complexes. Such aggregation simultaneously maximizes energy gain through both mechanisms. Indeed, based on measured electric properties, the formation of such aggregates has been postulated by Frank and Köstlin⁶ to occur at high tin-doping levels.

Given the apparent strong structural constraints regarding the relative positioning of Sn_{In} and O_i' —as expressed in the structure rules above—we can further speculate that such aggregation of defect clusters leads to highly ordered structures. It seems likely then that such ordered defect aggregates are precursors to the early (at relatively low tin-doping levels) precipitation of stoichiometric phases, such as $\text{In}_4\text{Sn}_3\text{O}_{12}$, which—similar to In_2O_3 —is derived from a fluorite-type lattice with structural vacancies in the oxygen sublattice and might well be considered an ordered defect structure of Sn-doped In_2O_3 . In this context, the above clustering rules appear to be obeyed in $\text{In}_4\text{Sn}_3\text{O}_{12}$: Nadaud *et al.*⁸ have found tin to occupy all the symmetric “b-like” sites, coordinated by six oxygen atoms, and one-third of the asymmetric “d-like” sites, coordinated by seven oxygen atoms. With d- and b-like-sites occupied by tin in $\text{In}_4\text{Sn}_3\text{O}_{12}$, the fact that the distribution of structural vacancies is such that the d-like-site is sevenfold and the b-like-site is sixfold coordinated, appears to follow from rule 1. Furthermore, in accordance with rules 2 and 3, two tin sites are not located on cation positions nearest to each other without at least one being seven coordinated.

(2) Atomistic Model: Defect Geometry and Relaxation

Tin substitution at indium sites leads to a distortion of the local geometry as a result of the somewhat smaller Sn^{4+} ion; thus, we find distances to the nearest oxygen atoms decreased. For the Sn(b) defect, all six oxygen atoms are at a distance of 2.08 Å, compared with 2.18 Å for In(b) in bulk In_2O_3 . The Sn(d) defect has oxygen atoms at distances of 2.04, 2.08, and 2.13 Å (two sites each); the distances around In(d) are 2.12, 2.20, and 2.22 Å. Thus, for the two types of Sn_{In} defects, we observe a uniform inward relaxation of the first coordination shell by ~ 0.1 Å, in agreement with what we would expect based on the ionic radii alone. For 6% ITO, tin-edge EXAFS analysis performed by Nadaud *et al.*⁸ finds an (averaged) inward relaxation of 0.18 Å.

Table VI. Calculated Position of the Oxygen Interstitial (O_i'') and Distances to Its Neighbors for Selected Defect Clusters[†]

Defect cluster	O_i'' position projected onto [111] (lattice units)	O_i'' distance to site [‡] (Å)		
		1st shell b-site (1 site)	1st shell d-site (3 sites)	2nd shell oxygen (6 sites)
O_i''	0.113	2.13	2.09	2.54–2.57
(Sn(d)· O_i)'	0.111	2.20	Sn: 2.01 In: 2.13 [‡]	2.47–2.59
(2Sn(d)· O_i) [×]	0.106	2.31	Sn: 2.05 [‡] In: 2.18	2.46–2.64
(3Sn(d)· O_i) [*]	0.102	2.39	Sn: 2.09	2.44–2.59
(Sn(b)· O_i)'	0.118	Sn: 2.04	2.14	2.47–2.55
(Sn(b)·Sn(d)· O_i) [×]	0.117	Sn: 2.09	Sn: 2.06 In: 2.19 [‡]	2.45–2.57
(3Sn(b) O_i) [*]	0.106	2.20	2.11	2.56–2.63
Experiment [§]	0.085	2.89	2.22	2.12–2.68

[†]Interstitial position is given as the average of its lattice coordinates $(x + y + z)/3$, i.e., in terms of the components of its projection onto the [111] axis. This is a suitable measure of O_i'' displacement toward the d-site cations (see text). [‡]Distances averaged over sites. [§]Reference 9.

Regarding the relaxations around isolated and clustered oxygen interstitials, we find the following (Table VI): For isolated O_i'' , distances to one In(b) and three In(d) sites in the first coordination shell are 2.13 and 2.09 Å, respectively, slightly smaller in comparison with the distances found for structural oxygen atoms (between 2.12 and 2.22 Å). When the interstitial is clustered with Sn_{In} , we find, as a general rule, a displacement of the interstitial toward the substituents (Sn_{In}) and away from nonsubstituted sites. For example, in the series of nearest-neighbor defect clusters O_i'' , (Sn(d)· O_i)', (2 Sn(d)· O_i)[×], and (3Sn(d)· O_i)^{*} (Table VI), an increase in the distance of the interstitial to In(b) from 2.13 to 2.39 Å is found; thus, O_i'' is increasingly pulled away from the nearest b-site cation and toward the plane formed by the three nearest d-site cations.

Experimental distances to nearest neighbors around O_i'' as well as the lattice position of the O_i have been reported in the Rietveld study of González *et al.*⁹ In all samples of oxidized and reduced ITO, O_i'' is located at lattice position $x = y = z = 0.085$ lattice units (see Fig. 1). Rather against intuition, their distance analysis has found the nearest neighbor of O_i'' to be another oxygen at a distance of 2.12 Å, with d-site cations only a little farther away at 2.22 Å.⁹ This indicates that the interstitial is much farther displaced along the $\langle 111 \rangle$ axis toward the plane of d-sites in comparison with what we find for isolated O_i'' . Our calculated interstitial lattice positions in Table VI (projected onto the $\langle 111 \rangle$ axis for ease of comparison with experiment) show that further displacement toward the d-site plane is possible when O_i'' is clustered with Sn_{In} . This is illustrated, for example, in clusters with substantial near-neighbor Sn(d) substitution as well as the low-energy 3:1 defect

cluster (3Sn(b)| O_i)^{*}; however, even in these clusters, the displacement is still far from the result of Ref. 9. From the results in Table VI, it is further evident that displacement away from the plane of d-sites relative to the isolated interstitial, that is, to lattice positions larger than $x = y = z = 0.113$ lattice units, occurs only in defect clusters with Sn(b) dopants in the first coordination shell. As discussed above, such clusters are energetically very unfavored and, therefore, unlikely to be formed. Overall, our results certainly support the idea of a net displacement of O_i'' toward the plane of d-sites when clustered with Sn_{In} .

(3) Density Functional Calculations

Embedded cluster density functional calculations were performed on selected defect clusters of Sn_{In} and O_i . For computational expediency, these calculations were limited to nearest-neighbor defect clusters; density functional calculations on defect clusters with Sn_{In} substitution in the second cation shell would have involved too many atoms to be practical.

By Mulliken analysis, we find partial atomic charges of approximately $Sn^{3.1+}$ and $In^{2.5+}$ with very little variation ($\Delta Q < 0.04e$) from one defect cluster to the next; thus, charges are somewhat below the ionic ideal of 4+ and 3+, respectively. The atomic charge of the interstitial oxygen—isolated as well as clustered with Sn_{In} —is about $-1.57e$, which is smaller than the charge of $-1.75e$ calculated for structural oxygen in In_2O_3 . This is further illustrated in Fig. 2 by the contour maps of electron density of defect clusters (Sn(b)· O_i)' and (Sn(d)· O_i)'. Displayed is the density in the Sn–

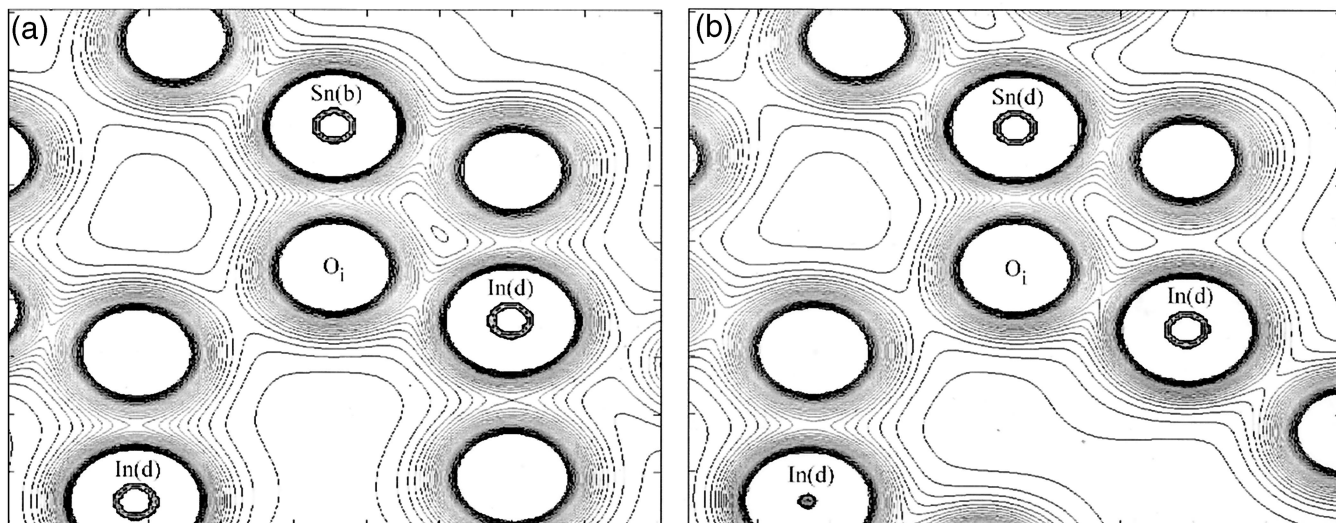


Fig. 2. Self-consistent valence electron densities from DV-X α embedded cluster calculations on defect clusters (a) (Sn(b)· O_i)' and (b) (Sn(d)· O_i)'.

Table VII. ^{119}Sn Mössbauer Parameters Calculated for Various Nearest-Neighbor Defect Clusters of Sn-Doped In_2O_3

Defect cluster	Site	Parameters [†]				
		$\rho(0)$ (e/a_0^3)	V_{zz} (a_0^{-3})	η	IS (mm/s)	QS (mm/s)
$\text{Sn}(b)^*$	Sn(b)	17.12	-0.44	-0.10	0.16	0.49
$\text{Sn}(d)^*$	Sn(d)	17.94	+0.94	-0.58	0.31	-0.97
$(\text{Sn}(b)\cdot\text{O}_i)'$	Sn(b)	16.58	-0.53	+0.15	0.05	0.58
$(\text{Sn}(d)\cdot\text{O}_i)'$	Sn(d)	17.81	+0.66	+0.27	0.29	-0.71
$(\text{Sn}(b)\cdot\text{Sn}(d)\cdot\text{O}_i)^\times$	Sn(b)	18.04	+0.43	+0.56	0.11	-0.44
	Sn(d)	16.86	+0.48	+0.01	0.33	-0.52
$(2\text{Sn}(d)\cdot\text{O}_i)^\times$	Sn(d)	17.99	+0.87	+0.36	0.32	-0.94
$(3\text{Sn}(d)\cdot\text{O}_i)^\times$	Sn(d)	18.25	+1.00	+0.40	0.37	-1.07
SnO_2^\ddagger	Sn	16.30	+1.10	+0.81	0.0	-1.07

[†] ρ_0 is the charge density at the nucleus, V_{zz} the principal component, η the asymmetry parameter of the electric-field gradient, IS the Mössbauer isomer shift, and QS the quadrupole splitting. [‡]Reference compound.

O_i -In plane of both defects. We note the presence of covalently shared charge of almost equal intensity between the interstitial oxygen and its tin and indium neighbors. In fact, without careful labeling of the atoms, it is practically impossible to tell which atom is tin and which is indium, which illustrates the electronic similarity of the two cations.

Calculated local charge distributions around Sn_{In} sites can be related to experimental ^{119}Sn Mössbauer isomer shifts (ISs) and quadrupole splittings (QSs) via the charge density and electric-field gradient at the nucleus, respectively. In Table VII, we have summarized our results of ^{119}Sn Mössbauer parameters for various point defects and defect clusters containing Sn_{In} sites. The QS for isolated Sn_{In} point defects at the b- and the d-sites have been calculated to be 0.49 and -0.97 mm/s, respectively. The approximate factor of 2 difference between the |QS| for the two sites is in qualitative agreement with the experimental result of Nadaud *et al.*,⁸ who found |QS| of 0.29 and 0.56 mm/s in ITO samples (0.5% tin) prepared under reducing conditions, which they assigned to b- and d-sites, respectively. Further quantitative comparisons between our data and the results of Ref. 8 are difficult to make, because experiment probes the average of all sites present and our calculations are limited to nearest-neighbor clusters. It is apparent, although, from the experimental results and our calculations, that, with increasing doping levels of Sn_{In} and O_i , considerable changes in QS and ISs occur. For example, we find for the series $(\text{Sn}(d)\cdot\text{O}_i)'$, $(2\text{Sn}(d)\cdot\text{O}_i)^\times$, and $(3\text{Sn}(d)\cdot\text{O}_i)^\times$ in Table VII that the IS and QS of Sn(d) sites increases with the number of Sn_{In} substitutions around an interstitial site.

IV. Conclusions

In this work, atomistic and density functional calculations have been used to explore clustering of oxygen interstitials (O_i^\bullet) with tin dopants ($\text{Sn}_{\text{In}}^\bullet$) in tin-doped indium oxide (ITO). A comprehensive survey of defect cluster structures involving up to three Sn_{In} sites in the first and second cation shells around a single oxygen interstitial found clustering of O_i^\bullet with $\text{Sn}_{\text{In}}^\bullet$ to be substantially favored. Based on calculated defect stabilization energies of the numerous structural combinations investigated, empirical rules for energetically favorable and unfavorable structures were proposed; in particular, our results indicate that the experimentally found b-site preference of tin dopants is not intrinsic to the point defect and is expressed only when clustered in nonnearest coordination with O_i^\bullet . For ITO of a doping ratio $\text{Sn}_{\text{In}}:\text{O}_i$ of 2:1, we find, in agreement with the Frank and Köstlin model,⁶ a strong preference to form neutral $[\text{2Sn}\cdot\text{O}_i]^\times$ defect clusters. Under reducing conditions, we find the formation of 3:1 clusters $[\text{3Sn}\cdot\text{O}_i]^\times$ to be thermodynamically favored; however, because of the relative immobility of $\text{Sn}_{\text{In}}^\bullet$, the formation of such clusters is unlikely at low doping levels. The energetics of defect clusters suggest that further stabilization is possible by aggregation into even larger clusters involving multiple oxygen interstitials and tin dopants. We further propose that the constraints expressed in our structure rules would

lead to a highly ordered aggregation, promoting an early precipitation of bixbyite-related stoichiometric phases, such as $\text{In}_4\text{Sn}_3\text{O}_{12}$, at low doping levels. Finally, density functional calculations on selected defect structures reveal that defect clustering leads to only small changes in partial atomic charges and bond orders but has a large effect on ^{119}Sn Mössbauer isomer shifts and quadrupole splittings.

Acknowledgment

We thank A. J. Freeman for a preprint of Ref. 16.

References

- C. G. Granqvist and A. Hultåker, "Transparent and Conducting ITO Films: New Developments and Applications," *Thin Solid Films*, **411**, 1-5 (2002).
- M. Marezio, "Refinement of the Crystal Structure of In_2O_3 at Two Wavelengths," *Acta Crystallogr.*, **20**, 723-28 (1966).
- A. J. C. Wilson (ed.), *International Tables for Crystallography*. Kluwer, Dordrecht, The Netherlands, 1992.
- E. C. Subbarao, P. H. Sutter, and J. Hrzio, "Defect Structure and Electrical Conductivity of ThO_2 - Y_2O_3 Solid Solutions," *J. Am. Ceram. Soc.* **48**, 443-46 (1965).
- H. Köstlin, R. Jost, and W. Lems, "Optical and Electrical Properties of Doped In_2O_3 Films," *Phys. Status Solidi A*, **29**, 87 (1975).
- G. Frank and H. Köstlin, "Electrical Properties and Defect Model of Tin-Doped Indium Oxide Layers," *Appl. Phys. A*, **27**, 197 (1982).
- J. H. Hwang, D. D. Edwards, D. R. Kammler, and T. O. Mason, "Point Defects and Electrical Properties of Sn-Doped In-Based Transparent Conducting Oxides," *Solid State Ionics*, **129**, 135-44 (2000).
- N. Nadaud, N. Leequeux, M. Nanot, J. Jové, and T. Roisnel, "Structural Studies of Tin-Doped Indium Oxide (ITO) and $\text{In}_4\text{Sn}_3\text{O}_{12}$," *J. Solid State Chem.*, **135**, 140 (1998).
- G. B. González, J. B. Cohen, J. H. Hwang, T. O. Mason, J. P. Hodges, and J. D. Jorgensen, "Neutron Diffraction Study of the Defect Structure of Indium-Tin-Oxide," *J. Appl. Phys.*, **89** [5] 2550-55 (2001).
- K. Nomura, Y. Ujihira, S. Tanaka, and K. Matsumoto, "Characterization and Estimation of ITO (Indium Tin Oxide) by Mössbauer Spectroscopy," *Hyperfine Interact.*, **42**, 1207-10 (1988).
- Z. M. Jarzelski, "Preparation and Physical Properties of Transparent Conducting Oxide Films," *Phys. Status Solidi A*, **71**, 13-41 (1982).
- J. C. C. Fan and J. B. Goodenough, "X-ray Photoemission Spectroscopy Studies of Sn-Doped Indium Oxide Films," *J. Appl. Phys.*, **48**, 3524-31 (1977).
- H. Odaka, S. Iwata, N. Taga, S. Ohnishi, Y. Kaneta, and Y. Shigesato, "Study on Electronic Structure and Optoelectronic Properties of Indium Oxide by First Principles Calculations," *Jpn. J. Appl. Phys.*, **36**, 5551-54 (1997).
- H. Odaka, Y. Shigesato, T. Murakami, and S. Iwata, "Electronic Structure Analyses of Sn-Doped In_2O_3 ," *Jpn. J. Appl. Phys.*, **40**, 3231-35 (2001).
- J. Tanaka, M. Mizuno, and H. Adachi, "Electronic Structure of Indium Oxide Using Cluster Calculations," *Phys. Rev. B: Condens. Matter*, **56**, 3536-39 (1997).
- O. N. Myrsov and A. J. Freeman, "Electronic Band Structure of Indium Tin Oxide and Criteria for Transparent Conducting Behaviour," *Phys. Rev. B: Condens. Matter*, **64**, 233111 (2001).
- O. Warschkow, D. E. Ellis, G. B. González, and T. O. Mason, "Defect Cluster Aggregation and Nonreducibility in Tin-Doped Indium Oxide," *J. Am. Ceram. Soc.*, **86** [10] 1707-11 (2003).
- J. D. Gale, "GULP (General Utility Lattice Program), A Computer Program for the Symmetry-Adapted Simulation of Solids," *J. Chem. Soc., Faraday Trans.*, **93**, 629 (1997).
- J. D. Gale, "Empirical Potential Derivation for Ionic Materials," *Philos. Mag. B*, **73**, 3 (1996).
- B. J. Dick and A. W. Overhauser, "Theory of the Dielectric Constants of Alkali Halide Crystals," *Phys. Rev.*, **112**, 90 (1958).
- T. S. Bush, J. D. Gale, C. R. A. Catlow, and P. D. Battle, "Self-Consistent Interatomic Potentials for the Simulation of Binary and Ternary Oxides," *J. Mater. Chem.*, **4**, 831-37 (1994).
- C. M. Freeman and C. R. A. Catlow, "A Computer Modeling Study of Defect and Dopant States in SnO_2 ," *J. Solid State Chem.*, **85**, 65-75 (1990).
- M. A. McCoy, R. W. Grimes, and W. E. Lee, "Planar Intergrowth in the $\text{ZnO-In}_2\text{O}_3$ System," *Philos. Mag. A*, **76**, 1187-201 (1997).
- M. F. Mott and M. J. Littleton, "Conduction in Polar Crystals: Electrolytic Conduction in Solid Salts," *Trans. Faraday Soc.*, **34**, 485 (1938).
- R. G. Parr and W. Yang, *Density Functional Theory of Atoms and Molecules*. Oxford University Press, New York, 1989.
- D. E. Ellis (ed.), *Electronic Density Functional Theory of Molecules, Clusters, and Solids*. Kluwer, Dordrecht, The Netherlands, 1995.
- D. E. Ellis and D. Guenzburger, "The Discrete Variational Method in Density Functional Theory and Its Applications to Large Molecules and Solid-State Systems," *Adv. Quantum Chem.*, **34**, 51-141 (1999).
- D. E. Ellis, G. A. Benesh, and E. Byrom, "Molecular Cluster Studies of Binary Alloys: LiAl ," *Phys. Rev. B: Solid State*, **16**, 3308-13 (1977).
- D. E. Ellis, G. A. Benesh, and E. Byrom, "Self-Consistent Embedded-Cluster Model for Magnetic Impurities: Fe, Co, and Ni in β -NiAl," *Phys. Rev. B: Condens. Matter*, **20**, 1198-207 (1979).
- J. Terra and D. Guenzburger, "Isomer Shifts and Chemical Bonding in Crystalline Sn(II) and Sn(IV)," *J. Phys.: Condens. Matter*, **3**, 6763-74 (1991).
- J. Terra and D. Guenzburger, "Electronic Structure and Electric-Field Gradients of Crystalline Sn(II) and Sn(IV) Compounds," *Phys. Rev. B: Condens. Matter*, **44**, 8584-98 (1991). □